The Canadian Mineralogist
Vol. 43, pp. 585-599 (2005)

CALDERITE-RICH GARNET AND FRANKLINITE-RICH SPINEL IN AMPHIBOLITE-FACIES HYDROTHERMAL SEDIMENTS, GAMSBERG Zn–Pb DEPOSIT, NAMAQUA PROVINCE, SOUTH AFRICA

Marcel STALDER and Abraham ROZENDAAL[§]

Department of Geology, University of Stellenbosch, Private Bag X1, Matieland 7602, South Africa

Abstract

Calderite-rich garnet and franklinite–jacobsite-rich spinel occur in amphibolite-facies hydrothermal metasedimentary rocks that stratigraphically overlie the Proterozoic Gamsberg Zn–Pb deposit, South Africa. The minerals are restricted in occurrence to an irregularly developed Mn–Fe-rich unit at the top of the ore-bearing horizon (the Gams Formation), which is interpreted to be genetically related to the underlying sulfide mineralization. The rocks are well laminated on a centimeter to decimeter scale and consist of alternating layers of garnet, pyroxenoid, Mn-rich clinopyroxene and Fe oxide (Zn–Mn-rich ferrite spinel, magnetite, hematite). The garnet contains up to 36% of the calderite component in solid solution with andradite and spessartine, whereas the spinel reaches a maximum franklinite component of 39% in solid solution with magnetite and jacobsite. Associated minor to accessory minerals include manganoan calcite, manganoan and zincian tremolite, Sr-rich epidote, hyalophane, pyrophanite, melanotekite and mimetite. The occurrence and spatial distribution of calderitic garnet, Zn–Mn-rich spinel and hematite constrain oxygen fugacities during metamorphism to conditions close to the HM buffer for the uppermost part of the Gams Formation, and indicate that considerable gradients in $f(O_2)$ and $f(S_2)$ existed within this specific horizon. The preserved assemblages are products of complex reduction and decarbonation reactions of protoliths composed of Mn–Ca-rich carbonate, Fe–Mn oxides and hydroxides, silica and aluminous clay. Under the observed conditions of P, T and $f(O_2)$, the contrasting parageneses are a function of delicate variations in the bulk composition of the precursor sediments. The Mn–Fe-rich and Zn–S-poor nature of these metahydrothermal rocks indicates that they represent a dispersion halo of low-temperature and oxidized fluids that postdated base-metal mineralization. Collectively, the unusual mineralogical and chemical composition of these rocks provides an indication of the spectrum of rock types that may be associated with metamorphosed deposits of base-metal sulfides.

Keywords: calderite-rich garnet, franklinite-rich spinel, pyroxenoids, manganese silicate rocks, Gamsberg deposit, South Africa.

Sommaire

Nous documentons la présence de grenat riche en caldérite et un spinelle riche en franklinite et en jacobsite dans les roches métasédimentaires d'origine hydrothermale, maintenant recristallisées au faciès amphibolite, qui reposent sur le gisement protérozoïque à Zn–Pb de Gamsberg, en Afrique du Sud. On ne trouve ces minéraux que dans une unité (la Formation Gams) enrichie en Mn–Fe développée de façon irrégulière dans la partie supérieure du niveau minéralisé; ce niveau aurait un lien génétique avec la minéralisation sous-jacente. Les roches sont bien laminées sur une échelle centimétrique ou décimétrique, et faites d'alternances de grenat, pyroxénoïde, clinopyroxène manganésifère, et oxydes de fer (spinelle ferrite à Zn–Mn, magnétite, hématite). Le grenat contient jusqu'à 36% du pôle caldérite en solution solide avec andradite et spessartine, tandis que le spinelle atteint un maximum de 39% du pôle franklinite dans une solution solide avec magnétite et jacobsite. Leurs sont associés les minéraux accessoires calcite manganésifère, trémolite manganésifère et zincifère, épidote riche en Sr, hyalophane, pyrophanite, mélanotékite et mimétite. La présence et la distribution du grenat caldéritique, du spinelle riche en Zn et Mn, et de l'hématite limitent la fugacité de l'oxygène au cours du métamorphisme à des conditions proches du tampon HM dans la partie supérieure de la Formation Gams, et témoignerait de gradients importants en $f(O_2)$ et $f(S_2)$. Les assemblages préservés résultent de réactions complexes de réduction et de décarbonatation des protolithes, contenant carbonate riche en Mn et Ca, oxydes et hydroxydes de Fe–Mn, silice et des argiles, sources d'aluminium. Aux conditions atteintes de P, T et $f(O_2)$, les paragenèses diverses reflètent des variations délicates en composition globale des sédiments précurseurs. Selon l'enrichissement en Mn et Fe et l'absence relative de Zn et de S, ces roches métahydrothermales représenteraient une auréole de dispersion de fluides de basse température et relativement oxydés qui circulaient suite à la minéralisation en métaux de base. Prises dans leur ensemble, les compositions minéralogique et chimique inhabituelles de ces roches fournissent une indication du spectre de lithologies qui peuvent être associées aux gisements de sulfures de métaux de base métamorphisés.

(Traduit par la Rédaction)

Mots-clés: grenat caldéritique, spinelle à franklinite, pyroxénoïdes, silicates de manganèse, gisement de Gamsberg, Afrique du Sud.

[§] *E-mail address*: ar@sun.ac.za

INTRODUCTION

Regionally metamorphosed sediment-hosted Zn–Pb deposits, such as at Broken Hill, Australia, and the famous Franklin and Sterling Hill deposits in New Jersey, are commonly hosted by unusual Fe–Mn–Ca–Si-rich metasedimentary units, which may both constrain the environment of deposition and provide guidelines for exploration (Plimer 1986, Johnson *et al.* 1990, Spry *et al.* 2000, Hitzman *et al.* 2003, Johnson & Skinner 2003). The origin of these rocks is believed to be intimately related to the process of base-metal mineralization and is attributed to mixing of oxidized hydrothermal constituents with detrital and chemical sediments of the depositional basin (Spry *et al.* 2000). Previous investigators also proposed a genetic relationship between these metahydrothermal rocks and Fe–Mn-rich metalliferous sediments (ochres and umbers) that are associated with modern hydrothermal vents (Johnson *et al.* 1990, Johnson & Skinner 2003).

The Gamsberg Zn–Pb deposit is one of four late Paleoproterozoic sediment-hosted base-metal deposits that occur in the central Namaqua Province of South Africa. In previous contributions, we described petrological and chemical characteristics of phosphatic iron formations and mineralized phosphorites, which are a diagnostic feature of the Gamsberg deposit (Stalder & Rozendaal 2002, 2004). In this paper, we report on a range of unusual Mn–Fe-rich assemblages that stratigraphically overlie the mineralized horizon and contain calderite-rich garnet and Zn–Mn-rich ferrite spinel as major components. These minerals are relatively rare and restricted in occurrence to metamorphosed rocks with unusual bulk-compositions and generally high levels of oxidation. Pure calderite ($Mn_3Fe_2Si_3O_{12}$) is as yet unknown in nature, but garnet containing between 25 and 70% of the calderite component has been described from Mn^{2+}–Fe^{3+}-rich metasedimentary units (Klein 1966, Dasgupta *et al.* 1987, Reinecke 1987, Bühn *et al.* 1995). In these rocks, calderitic garnet occurs associated with minerals such as rhodonite, aegirine, tephroite, braunite, jacobsite, hausmannite, hematite, rhodochrosite, calcite and quartz. Franklinite (ideally, $ZnFe_2O_4$) is most notably found in the metamorphosed Zn–Fe–Mn deposits of Franklin and Sterling Hill, where it formed one of the main ore minerals (Frondel & Klein 1965, Johnson *et al.* 1990). The mineral has also been described from several localities in the Bergslagen Province of central Sweden (Burke & Kieft 1972, Holtstam 2002), and minor occurrences elsewhere (Anthony *et al*. 1997).

GEOLOGICAL SETTING AND OCCURRENCE

The Gamsberg Zn–Pb deposit (150 Mt at 7% Zn and 0.5% Pb) is situated near the Northern Cape mining town of Aggeneys, in the central part of the Namaqua Province of South Africa (Fig. 1a). Country rocks in the area belong to the late Paleoproterozoic (2000–1600 Ma) Bushmanland Group, a multiply deformed and metamorphosed volcano-sedimentary sequence composed of quartzite, metapelitic to metapsammitic schist and amphibolite that overlie a suite of quartz–feldspar gneiss (Rozendaal 1986, Moore *et al*. 1990).

The Gamsberg deposit occurs within a large sheath-fold structure that has been exposed as a prominent inselberg (Fig. 1b). The ore-bearing horizon is referred to as the Gams Formation and consists of a sequence of metalliferous metasedimentary rocks and interbedded metapelite up to 100 m thick (Rozendaal & Stumpfl 1984, Rozendaal 1986). The Gams Formation is subdivided into several units. Base-metal and Fe sulfides are mostly confined to quartz – sillimanite – muscovite – graphite and quartz – garnet – amphibole rocks of the central B unit. The latter is enveloped by a heterogeneous sequence of Fe–Mn–Ca-rich silicate-, carbonate- and oxide-facies metasedimentary rocks of the A and C units (Fig. 2). Calderitic garnet and franklinitic spinel are restricted to the irregularly developed C2 unit (0–15 m thick) at the top of the Gams Formation. The C2 unit consists of distinctly laminated Mn–Fe-rich rocks composed of yellow garnet-rich layers that alternate with pinkish pyroxenoid-rich layers and black Fe–Mn(–Zn) oxide layers (Fig. 3). The absence of sulfide minerals and the predominance of Mn^{2+}- and Fe^{3+}-rich silicate and oxide minerals suggest higher $f(O_2)$ and corresponding lower $f(S_2)$ conditions in this unit than in the underlying ore-bearing units.

The Gamsberg orebody and associated metalliferous host-rocks have been multiply deformed and metamorphosed along with the country rocks during the Kibaran and Namaquan orogenic events from 1220–1170 Ma and 1060–1030 Ma, respectively (Thomas *et al.* 1994, Robb *et al.* 1999). At least three phases of deformation are recognized, with the main fabric-forming event (D_2) being represented by east–west-trending recumbent isoclinal folds (F_2). These structures were reworked by east–west-trending open folds (F_3) on a kilometer-scale wavelength, and later thrusts and shear zones that developed during subsequent compressional events (D_3–D_4). Conditions of metamorphism in the area are constrained by the presence of the assemblages cordierite + sillimanite + K-feldspar and quartz + muscovite in metapelite, with P–T estimates ranging from 630 to 670°C and 3 to 4.5 kbar (Joubert 1986, Rozendaal 1986). Textural evidence indicates that the peak conditions of metamorphism were contemporaneous with and outlasted D_2, but were terminated before the onset of D_3. On a regional scale, retrograde metamorphic effects are reflected by epidote formation at the expense of amphibole, the development of chlorite along existing foliation planes, and newly recrystallized quartz in the late shear fabrics (Joubert 1986).

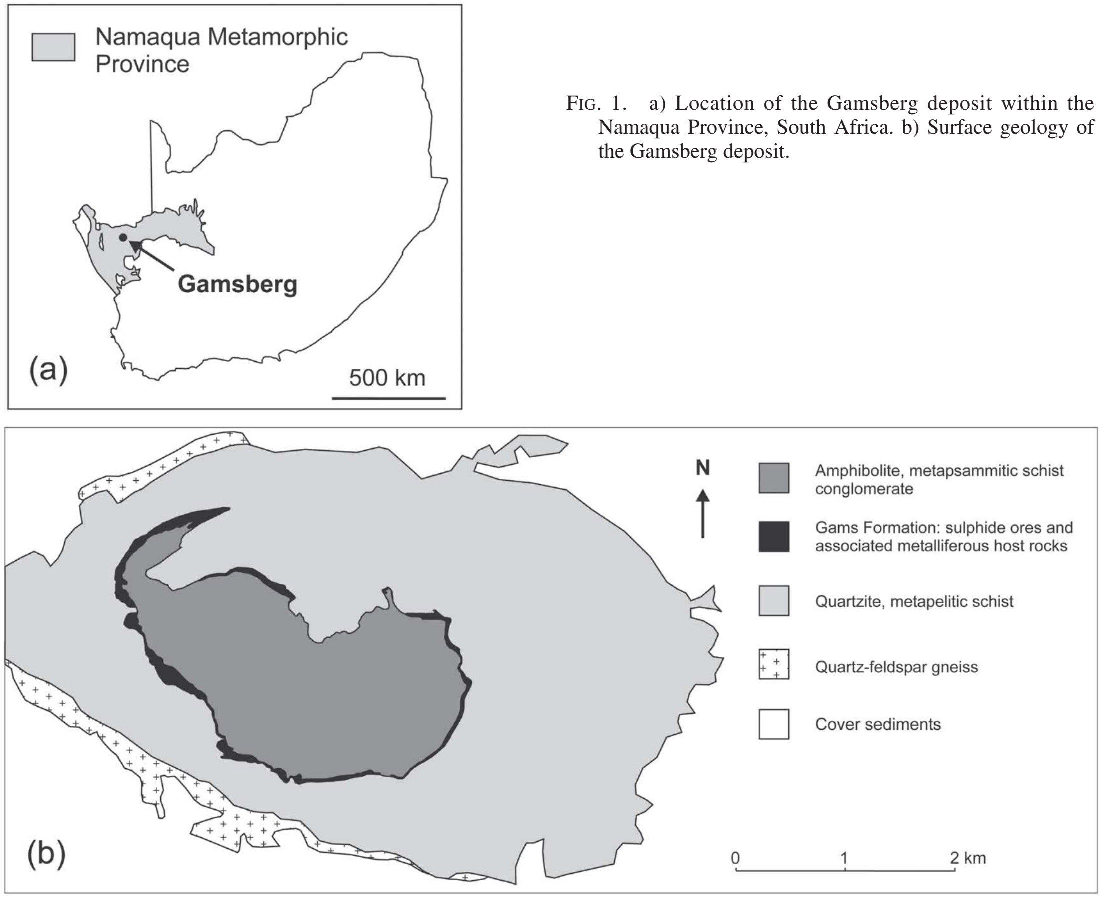

FIG. 1. a) Location of the Gamsberg deposit within the Namaqua Province, South Africa. b) Surface geology of the Gamsberg deposit.

PETROGRAPHY AND TEXTURAL RELATIONSHIPS

Characteristic assemblages of the C2 unit are listed in Table 1, and typical microtextures are presented in Figures 4, 5 and 6. The major minerals are medium- to coarse-grained and meet at triple junctions, indicating that they represent equilibrium metamorphic assemblages. The assemblages have been subdivided into three types, depending on the nature of the associated Fe oxide: (i) assemblages that contain Mn–Zn-rich ferrite spinel, (ii) assemblages that contain Mn–Zn-poor magnetite, and (iii) assemblages that contain hematite.

Garnet forms the dominant mineral in most assemblages. It has a characteristic bright yellow to brownish color in thin section and shows slight anisotropism along grains boundaries. The mineral occurs as massive granoblastic aggregates (Figs. 4a, b) and individual subhedral to euhedral grains that range in size from 0.1 to 2 mm. In the southern part of Gamsberg, the C2 unit is dominated by massive, fine-grained garnet–quartz–hematite rocks (sample G77–632). Garnet is commonly poikiloblastic and contains inclusions of quartz, K-feldspar, magnetite or franklinite-rich and jacobsite-rich spinel (Figs. 4c, 5c). In some assemblages (*e.g.*, GR–65), garnet displays a "honey-comb" texture owing to the coalescence of individual grains of atoll garnet (Figs. 5a, b). The occurrence of relict cores of garnet within clinopyroxene and pseudomorphs of clinopyroxene after garnet suggest that garnet has been altered to clinopyroxene during retrograde metamorphism (Burton *et al.* 1982). Additional textural evidence for the breakdown of garnet includes its alteration to a mixture of Sr-rich epidote, pyrophyllite and quartz.

Franklinite- and jacobsite-rich spinel has been observed in three samples (G38–1080, G74–680 and G111–284), where it occurs together with garnet, manganoan calcite, clinopyroxene or rhodonite. It is present as medium- to coarse-grained (<2 mm) annealed grains and aggregates that are commonly concentrated within individual microbands (<1 cm). Inclusions of garnet are common in spinel and *vice versa*, suggesting simultaneous crystallization of the two minerals. Back-scattered electron images illustrate that the Zn–Mn-rich spinel from Gamsberg is chemically homogeneous, and no exsolution lamellae or intergrowths with magnetite or pyrophanite ($MnTiO_3$) have been observed (Fig. 6). Complex intergrowths of franklinite with these minerals are a common feature at the Franklin and Sterling Hill deposits, and have been interpreted as reflecting unmixing of these phases during slow cooling (Frondel & Klein 1965, Valentino *et al*. 1990). Ferrite spinel shows signs of brittle fracture along the {111} cleavage (Fig. 6a), especially where individual grains have been tectonically forced against each other. Individual grains in sample G38–1080 are characterized by a homogeneous core and altered rim (Fig. 6b), indicating that conversion of magnetite to hematite has occurred.

In type (ii) assemblages, the dominant oxide mineral is magnetite with low Mn and Zn contents. Magnetite occurs as annealed aggregates in distinct microlayers or as individual porphyroblasts associated with garnet, pyroxenoid, clinopyroxene, manganoan calcite and lesser amounts of K-feldspar and biotite. In contrast to Zn–Mn-rich spinel, magnetite normally contains blebs and lamellae of pyrophanite. The latter occurs exclusively within magnetite, suggesting that it represents a product of exsolution of an original Mn-enriched spinel. Hematite is restricted to type (iii) assemblages and occurs as small euhedral grains that are normally concentrated in individual seams (<1 mm).

Pyroxenoid minerals (rhodonite and pyroxmangite) may occur in all three types of assemblages and are present as individual medium-grained prismatic grains (0.5–2 mm) in association with garnet, spinel, quartz or manganoan calcite (Figs. 4d, 5d). As in the case of garnet and spinel, the pyroxenoids are commonly concentrated within separate mesobands 2 to 5 cm thick. Clinopyroxene is present as a major component in type (i) and (ii) assemblages, where it is normally intimately

TABLE 1. MINERAL ASSEMBLAGES TYPICAL OF THE C2 UNIT

Sample	Mineralogy (major, *minor and accessory*)
	Type (i) assemblages
G38–1080	garnet^{1} + spinel^{3} + manganoan calcite + *manganoan tremolite* + *melanotekite* + *apatite*
G74–680	garnet^{1} + spinel^{3} + rhodonite
G111–284	garnet^{1} + clinopyroxene + spinel^{3} + hyalophane + *melanotekite*
	Type (ii) assemblages
G39–917	garnet^{1} + rhodonite + manganoan calcite + spinel^{4} + clinopyroxene + *K-feldspar* + *pyrophanite*
G76–496	garnet^{2} + pyroxmangite + spinel^{4} + *pyrophanite*
G109–88	clinopyroxene + rhodonite + garnet^{2} + *biotite* + *K-feldspar* + *spinel*^{4} + *pyrophanite*
G118–188	clinopyroxene + garnet^{2} + rhodonite + spinel^{4} + *pyrophanite*
	Type (iii) assemblages
G64–740	garnet^{1} + rhodonite + quartz + hematite + *manganoan tremolite* + *melanotekite* + *mimetite*
G77–632	garnet^{2} + quartz + hematite + *manganoan calcite*
GR–65	garnet^{2} + quartz + hematite + epidote + pyrophyllite + clinopyroxene + mimetite + apatite

1: andradite–calderite-dominant (> 50% andradite + calderite)
2: spessartine-dominant (> 50% spessartine)
3: Zn–Mn-rich ferrite spinel
4: magnetite

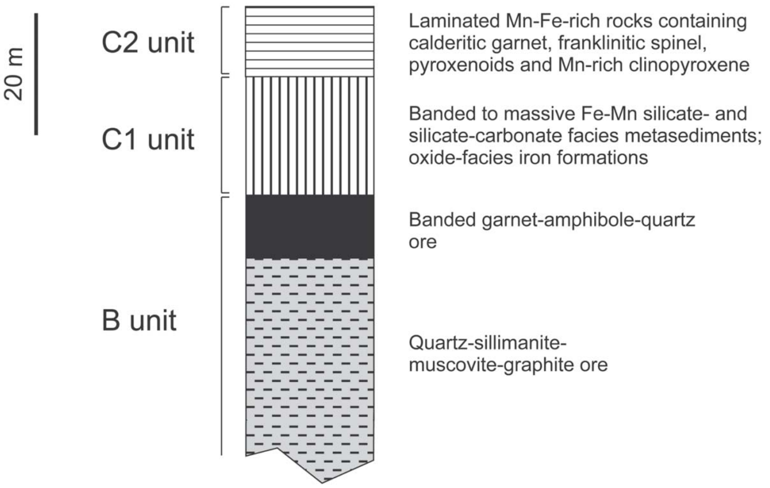

FIG. 2. Schematic section of the upper parts of the Gams Formation showing the distribution of ores and metalliferous host-rocks.

associated with rhodonite. Two generations of clinopyroxene have been identified on textural and chemical evidence. Clinopyroxene 1 occurs as medium-grained individual crystals or intergrown clusters in samples G111–284 and G118–188. As in the case of other prograde minerals, it is commonly concentrated in individual mesobands (Fig. 4b). The second generation of clinopyroxene is found in samples G39–917 and G109–88 and occurs as individual roundish grains and pseudomorphs after garnet. Both clinopyroxenes 1 and 2 are brownish to greenish brown in thin section and display slight pleochroism.

Associated minor and accessory minerals include manganoan calcite, quartz, Mn–Zn-rich tremolite, Ba-bearing K-feldspar, biotite, melanotekite ($Pb_2Fe^{3+}_2 Si_2O_9$), pyrophanite, apatite, and small scattered grains of mimetite, $Pb_5(AsO_4)_3Cl$. Quartz is restricted to type (iii) assemblages that contain hematite. The preservation of manganoan calcite in some samples (*e.g.,* G38–1080, G39–917) indicates that $f(CO_2)$ has locally been high enough to prevent total consumption of carbonate in prograde decarbonation-type reactions. Melanotekite is a rare Pb-silicate that has most notably been described from its type locality at Långban, Sweden (*e.g*., Glasser 1967). In the microscope, it shows greenish yellow to yellow-brown pleochroism and occurs as isolated grains or small patches that are intimately associated with garnet.

GEOCHEMICAL RESULTS

Analytical techniques and formula calculation

Whole-rock chemical compositions of the manganiferous assemblages were obtained using standard methods of X-ray fluorescence (XRF) with a Philips PW 1404 wavelength-dispersion spectrometer at the University of Stellenbosch.

The franklinite-rich spinel has been identified by X-ray diffraction (XRD) using a Philips PW 1130 diffractometer at the University of Stellenbosch. The mineral is strongly magnetic and can be easily separated from crushed rocks by means of a hand magnet. The individual minerals were analyzed with an electron microprobe using a JEOL Superprobe 733 at Rhodes University, Grahamstown. Analyses were run with an acceleration voltage of 20 kV and a beam current of 30 nA. The following standards were used: pyrope (Si, Mg), rutile (Ti), almandine (Fe, Al), rhodonite (Mn), willemite (Zn), diopside (Ca), albite (Na), orthoclase (K), sanidine (Ba), $SrTiO_3$ (Sr) and crocoite (Pb). For the analysis of spinel, magnetite was used as a standard for Fe. Detection limits were found to be (in wt.%): Na_2O, K_2O: 0.02, MnO: 0.03, SiO_2, Al_2O_3, FeO, ZnO: 0.05, MgO, TiO_2: 0.06, SrO: 0.08, BaO: 0.10, and PbO: 0.24. The amount of Fe^{3+} in the spinel and garnet was calculated from electron-microprobe results using criteria of stoichiometry (Droop 1987). Manganese has been regarded as divalent owing to stoichiometric considerations and the absence of Mn^{3+}-bearing minerals at Gamsberg. Garnet end-members were assigned according to the following procedure: 1) Mg and Fe^{2+} to pyrope and almandine, respectively, 2) all Al to spessartine, 3) all Ca to andradite, 4) remaining Mn and Fe^{3+} to calderite.

Back-scattered electron images of spinel were obtained using a Leo 1430VP scanning electron microscope with a Centaurus detector mounted below the pole piece, at the University of Stellenbosch. Operating conditions were: accelerating voltage 25 kV, probe current 391 pA, and a working distance of 12.8 mm.

Mineral compositions

The compositions of garnet, spinel, pyroxenoid and clinopyroxene are plotted in Figures 7–10, and representative compositions are listed in Tables 2–4. Garnet from the C2 unit is essentially a solid solution among andradite, calderite and spessartine (Fig. 7). Most of the Fe is trivalent, substituting for Al in the octahedral position, whereas the dodecahedral position is predominantly occupied by Mn and Ca. The composition of the investigated garnet varies in the range delimited by $Adr_{46}Sps_{37}Cdr_{12}$, $Cdr_{36}Adr_{35}Sps_{23}$ and $Sps_{69}Adr_{17} Alm_{10}$, corresponding to maximum andradite (Adr), calderite (Cdr) and spessartine (Sps) components, respectively. The composition of the Gamsberg garnet compares well with most examples of calderite-rich garnet from the literature, although Klein (1966) presented two garnet compositions that contain 57 and 69% of the calderite component. As noted by Lattard & Schreyer (1983), however, the structural formula of these samples is not stoichiometric, and levels of Mg and Al were not established. At Gamsberg, andradite–calderite-dominant garnet occurs in all three types of assemblages, whereas spessartine-dominant garnet is restricted to type (ii) and (iii) assemblages. The garnet in association with manganoan calcite is enriched in the andradite component (G38–1080, G39–917), compared to garnet in carbonate-free assemblages.

The Gamsberg ferrite spinel is a solid solution among magnetite, jacobsite and franklinite (Fig. 8). Zinc concentrations range from below 1 wt.% ZnO in type (ii) assemblages to a maximum of 13.79 wt.% in sample G111–284 (39 mole % franklinite). Franklinite-bearing spinel from Gamsberg is rich in Mn and Fe^{2+}, reaching a maximum of 48 mole % jacobsite and 61 mole % magnetite, respectively. Ferroan franklinite has also been reported from Franklin and Sterling Hill, where it is referred to as "magnetic franklinite" (Frondel & Klein 1965, Johnson *et al.* 1990, Sclar & Leonard 1992). Near-end-member franklinite has been reported from Bergslagen, Sweden (Holtstam 2002).

Rhodonite and pyroxmangite are distinguished by the larger 2*V* and higher Ca content of the former (Fig. 9). The pyroxenoids are Mn-rich, reaching a maxi-

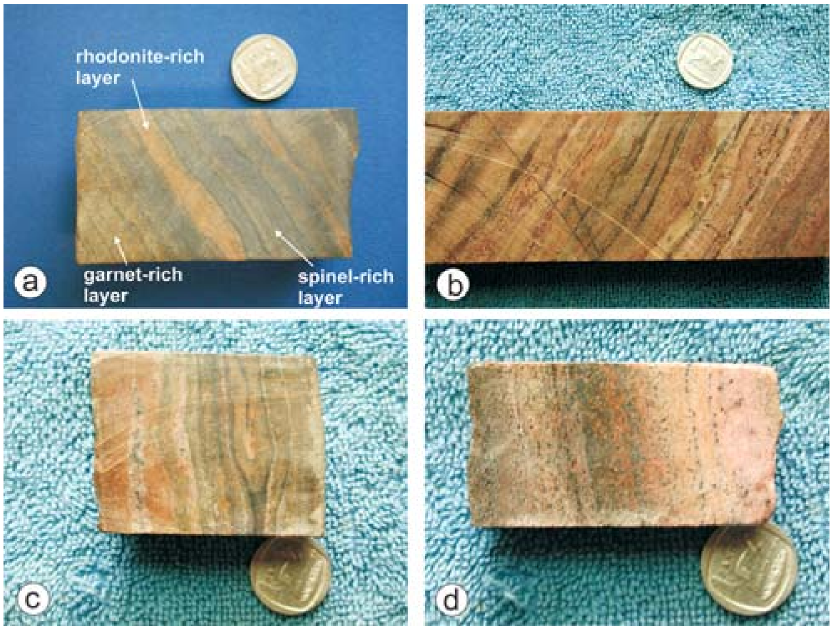

FIG. 3. Drillhole core-intervals showing typical rock-types of the C2 unit. a–c) Banded garnet – spinel – pyroxenoid rocks. d) Layers of pinkish rhodonite alternating with dark spinel-rich layers.

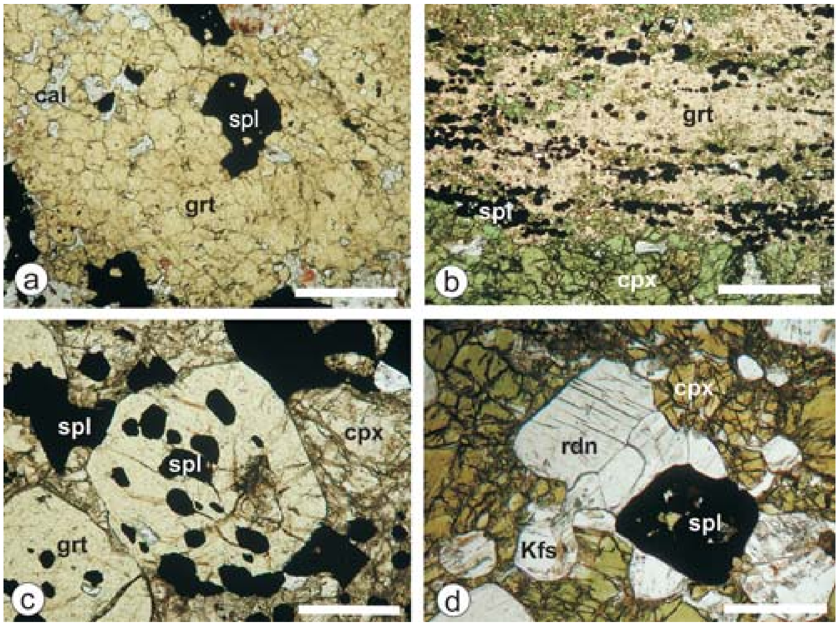

Fig. 4. Photomicrographs showing textural relationships of the assemblages in the C2 unit. a) Mn–Zn-rich ferrite spinel embedded in massive granoblastic garnet and interstitial manganoan calcite (sample G38–1080). b) Banded garnet – clinopyroxene – spinel rock composed of layers of massive yellow garnet alternating with layers of green clinopyroxene and seams of ferrite spinel (sample G118–188). c) Garnet poikiloblast containing inclusions of Zn-rich ferrite spinel in association with clinopyroxene (sample G111–284). d) Euhedral rhodonite in association with manganoan clinopyroxene, ferrite spinel and K-feldspar (sample G39–917). Scale bars represent 0.5 mm. Mineral abbreviations: cal: calcite, cpx: clinopyroxene, grt: garnet, Kfs: K-feldspar, rdn: rhodonite, spl: spinel.

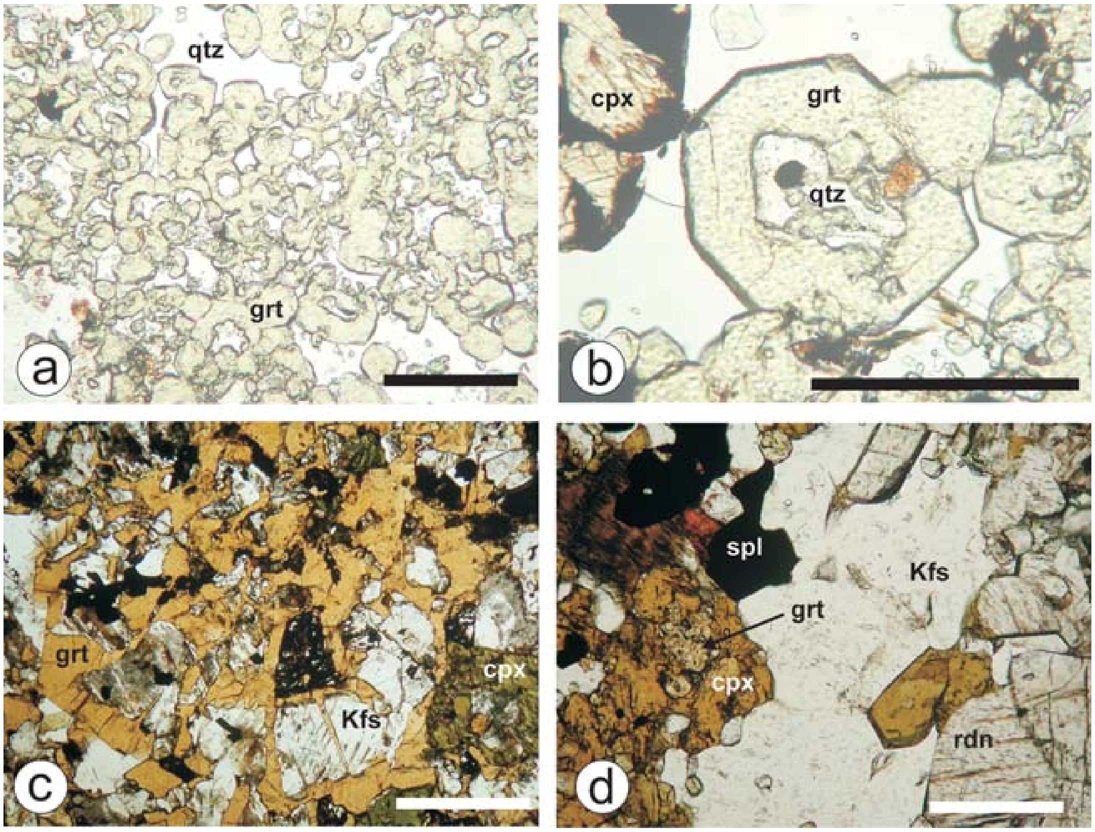

FIG. 5. Photomicrographs showing textural relationships of garnet. a) "Honeycomb" texture owing to the coalescence of individual grains of atoll garnet (sample GR–65). b) Close-up of individual atoll garnet enclosing core of quartz (sample GR–65). c) Large poikiloblast of garnet enclosing K-feldspar (sample G39–917). d) Relics of garnet within clinopyroxene attest to the alteration of garnet to clinopyroxene (sample G109–88). Scale bars represent 0.5 mm. Mineral abbreviations: qtz: quartz; for other abbreviations, see Figure 4.

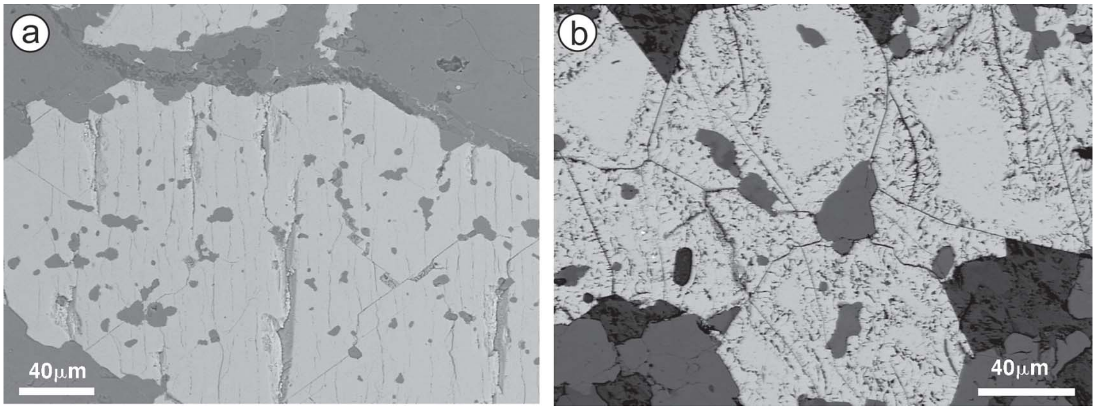

FIG. 6. Back-scattered electron images of franklinite-rich spinel. a) Franklinite-rich spinel with garnet inclusions in a matrix of garnet (sample G74–680). The grain shows signs of brittle deformation along the {111} cleavage. b) Jacobsite–franklinite aggregates in a matrix of garnet and manganoan calcite (sample G38–1080). Individual grains display signs of conversion to hematite.

mum of 76 mole % $MnSiO_3$. The pyroxenoid in association with spinel is relatively enriched in Fe, whereas that in association with hematite is depleted in Fe. In type (ii) and (iii) assemblages, pyroxenoid may be enriched in Zn (up to 1.28 wt.% ZnO), suggesting that the available Zn is incorporated into the silicate structures in assemblages where a franklinitic spinel is not stable. The clinopyroxene is a solid solution among hedenbergite, diopside and johannsenite (Fig. 10). The composition ranges in the interval defined by $Hd_{53}Jh_{24}Di_{23}$, $Di_{56}Jh_{25}Hd_{19}$ and $Hd_{43}Jh_{29}Di_{28}$, corresponding to maximum hedenbergite (Hd), diopside (Di) and johannsenite (Jh) components, respectively. Clinopyroxene 2 is enriched in Na and Mn relative to clinopyroxene (Table 4). Cation proportions in the former consistently deviate from stoichiometry, suggesting that the mineral has not totally equilibrated.

Selected compositions of minor and accessory minerals are presented in Table 5. The compositions of carbonate and amphibole correspond to manganoan calcite and manganoan tremolite, respectively. The latter may contain up to 1.4 wt.% ZnO. Melanotekite is poor in Mn, demonstrating limited solid-solution toward the Mn^{3+} end-member kentrolite. Similarly, pyrophanite is close to its end-member composition. Epidote is enriched in Sr, reaching a maximum of 15.83 wt.% SrO (0.827 *apfu*). Manganese concentrations are low; solid solution toward piemontite thus is limited. Unlike the latter, which may contain considerable Sr, reports of strontian epidote are rare in the literature. Grapes & Watanabe (1984) described epidote containing up to 8.5 wt.% SrO. To the authors' knowledge, the Gamsberg epidote represents the most Sr-rich epidote reported thus far. The epidote also contains minor Pb, and thus contains a minor amount of the hancockite component. The Gamsberg K-feldspar may contain considerable Ba. In sample G111–284, the feldspar contains around 25% of the celsian component, thus corresponding to the intermediate member hyalophane.

Bulk composition of the manganiferous assemblages

The bulk composition of selected assemblages is listed in Table 6. The chemical composition of the rocks is mostly a function of variation in the concentrations of Si, Fe, Mn, Ca and Al. Andradite–calderite-bearing rocks are characterized by low concentrations of chemically immobile Al and Ti, as well as high Mn:Al ratios (>4.2). Assemblages containing the most calderite-rich garnet (G74–680 and G64–740) have Mn:Al ratios in excess of 8. In contrast, rocks that contain spessartine-dominant garnet are enriched in Al and Ti and have Mn:Al ratios below 3.36 (GR–65, G77–632).

Type (i) assemblages that contain franklinitic and jacobsitic spinel are relatively enriched in Fe and de-

TABLE 2. REPRESENTATIVE COMPOSITIONS OF GARNET

Sample	G74-680	G64-740	G111-284	G76-496	G39-917	G109-88	G38-1080	G77-732
SiO_2 wt.%	34.68	34.52	35.13	35.25	34.87	35.44	35.73	36.22
TiO_2	0.15	0.09	0.23	0.23	n.d.	0.15	0.13	n.d.
Al_2O_3	5.70	5.67	8.77	13.63	5.41	12.25	8.63	16.48
Fe_2O_3*	21.45	22.00	16.83	9.42	22.73	12.18	18.15	6.24
FeO	2.50	2.36	2.84	4.42	3.03	2.99	2.28	4.29
MnO	24.00	23.29	27.60	34.07	16.28	30.53	20.32	30.30
MgO	0.05	0.08	0.13	n.d.	n.d.	n.d.	0.16	0.46
CaO	11.37	11.86	8.57	2.52	17.32	6.61	15.28	5.88
Total	99.89	99.87	100.11	99.54	99.64	100.15	100.68	99.87
Si *apfu*	3.004	2.990	3.006	3.004	2.993	2.996	2.996	3.001
Ti	0.010	0.006	0.015	0.015	0.000	0.010	0.008	0.000
Al	0.582	0.579	0.884	1.368	0.547	1.221	0.853	1.609
Fe^{3+}	1.398	1.434	1.084	0.604	1.468	0.775	1.145	0.389
Fe^{2+}	0.181	0.171	0.203	0.315	0.217	0.211	0.160	0.297
Mn	1.761	1.709	2.000	2.458	1.183	2.186	1.443	2.126
Mg	0.006	0.010	0.016	0.000	0.000	0.000	0.020	0.056
Ca	1.055	1.100	0.786	0.230	1.592	0.599	1.373	0.521
Andradite	35.1	36.8	26.1	7.7	53.2	20.0	45.8	17.0
Pyrope	0.2	0.3	0.5	0.0	0.0	0.0	0.7	1.8
Spessartine	22.8	23.0	36.8	57.9	20.2	54.1	36.7	69.4
Grossular	0.0	0.0	0.0	0.0	0.0	0.0	0.0	0.0
Almandine	6.0	5.7	6.8	10.5	7.3	7.1	5.3	9.7
Calderite	35.8	34.2	29.7	24.0	19.4	18.9	11.5	2.0

Notes: n.d.: not detected. * The proportion of Fe_2O_3 is calculated from stoichiometry. Results of all analyses were normalized to 12 atoms of oxygen; cation proportions are expressed in atoms per formula unit (*apfu*). Proportions of the components are expressed in mol.%.

TABLE 3. REPRESENTATIVE COMPOSITIONS OF FERRITE SPINEL

Sample	G111-284		G74-680		G38-1080		G109-88	G39-917
SiO_2 wt.%	n.d.	n.d.	n.d.	n.d.	n.d.	n.d.	n.d.	0.06
TiO_2	0.30	0.20	0.24	0.24	0.25	0.11	0.06	0.30
Al_2O_3	1.24	1.56	0.31	0.30	0.19	0.19	0.13	0.07
Fe_2O_3*	66.35	65.76	68.28	67.61	68.84	67.75	68.43	68.28
FeO	7.51	6.62	7.14	13.51	18.87	13.74	26.56	30.01
MnO	11.44	14.48	14.50	8.13	9.21	13.89	4.12	0.40
MgO	n.d.	n.d.	0.39	0.48	0.42	0.17	n.d.	0.49
CaO	n.d.	n.d.	n.d.	n.d.	n.d.	n.d.	n.d.	n.d.
ZnO	13.79	11.05	10.02	9.62	3.06	3.03	0.29	0.21
Total	100.63	99.67	100.89	99.89	100.84	98.88	99.58	99.82
Si *apfu*	0.000	0.000	0.000	0.000	0.000	0.000	0.000	0.002
Ti	0.009	0.006	0.007	0.007	0.007	0.003	0.002	0.009
Al	0.056	0.071	0.014	0.014	0.009	0.009	0.006	0.003
Fe^{3+}	1.926	1.917	1.972	1.966	1.976	1.985	1.991	1.974
Fe^{2+}	0.242	0.215	0.229	0.437	0.602	0.448	0.859	0.964
Mn	0.374	0.475	0.471	0.266	0.297	0.458	0.135	0.013
Mg	0.000	0.000	0.022	0.028	0.024	0.010	0.000	0.028
Ca	0.000	0.000	0.000	0.000	0.000	0.000	0.000	0.000
Zn	0.393	0.316	0.284	0.286	0.086	0.087	0.008	0.006
Magnetite	24.02	21.34	23.29	44.17	61.08	45.08	85.72	98.07
Jacobsite	37.05	47.23	47.88	26.91	30.18	46.15	13.46	1.32
Franklinite	38.93	31.43	28.84	28.92	8.74	8.78	0.82	0.61

Notes: n.d.: not detected. * The proportion of Fe_2O_3 is calculated from stoichiometry. Results of all analyses were normalized to three cations; cation proportions are expressed in atoms per formula unit (*apfu*). Proportions of the components are expressed in mol.%.

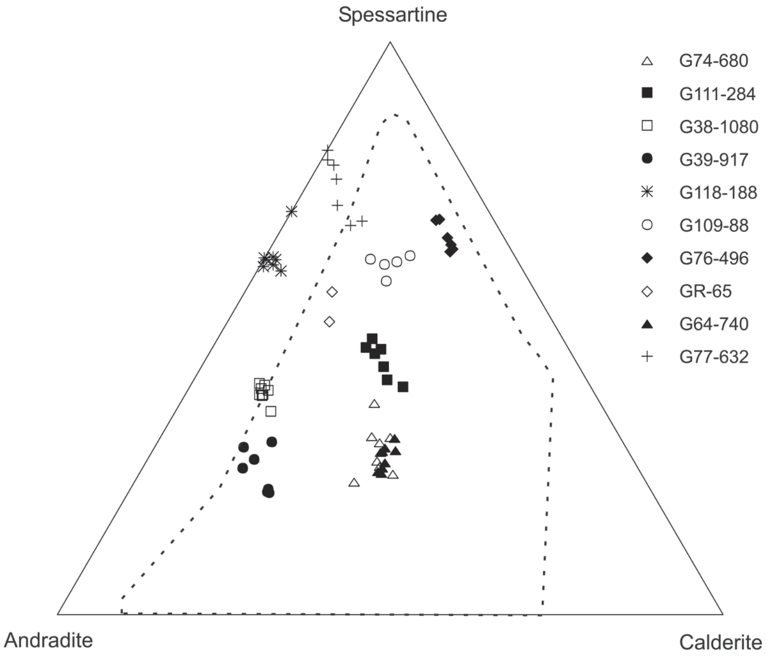

FIG. 7. Compositions of the garnet in the assemblages investigated in the C2 unit. The stippled line denotes the compositional range of calderite-bearing garnet from the literature. Data from Klein (1966), Dasgupta *et al.* (1987), Reinecke (1987), Jiménez-Millán & Velilla (1994), and Bühn *et al.* (1995).

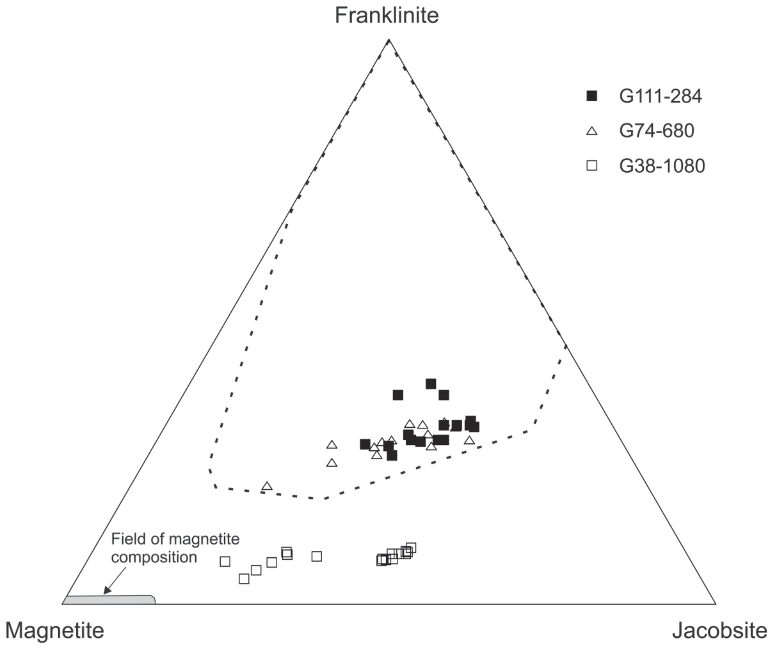

FIG. 8. Composition of ferrite spinel in the C2 unit. The stippled field corresponds to the composition of franklinite-rich spinel reported in the literature. Data from Frondel & Klein (1965), Johnson *et al.* (1990), and Holtstam (2002).

pleted in Si compared to type (ii) and (iii) assemblages. The Fe:Si ratio in the former is between 1.75 and 2.82, whereas magnetite- and hematite-bearing assemblages have a Fe:Si ratio below 1. In addition, assemblages that contain Zn–Mn-rich spinel have relatively low Mn/Fe values. Type (iii) assemblages that contain hematite and quartz are enriched in SiO_2 and display high Si/(Si + Mn) values compared to the other assemblages. Rhodonite is stable in assemblages with Mn/Al > 8 and Si/(Si + Mn) values between 0.5 and 0.6. Assemblages with Si/(Si + Mn) values above 0.6 are characterized by the paragenesis garnet + hematite + quartz (samples GR–65 and G77–632), whereas those with Si/(Si + Mn) values below 0.5 contain garnet + spinel + carbonate.

All assemblages are anomalously enriched in Zn and Pb, and to a lesser degree in Ba, Sr and As, compared to related rock-types such as Algoma-type iron formations and exhalative manganese formations (Ashley 1989, Dasgupta *et al.* 1990, Bühn *et al.* 1995, Spry *et al.* 2000).

CONSTRAINTS ON THE OXYGEN FUGACITIES

The bulk compositions and observed parageneses demonstrate that the C2 unit has been metamorphosed under $f(O_2)$ conditions where all the Mn is divalent and most of the Fe trivalent. The close association of hematite-bearing and magnetite-bearing mineral assemblages suggests layer-to-layer variation in oxygen fugacity and indicates that oxygen behaved conservatively during metamorphism.

An upper limit of $f(O_2)$ is constrained by the absence of Mn^{3+}-bearing minerals at Gamsberg, which places the assemblages below the "rhodonite – braunite – quartz" buffer of Abs-Wurmbach & Peters (1999) (Fig. 11). At $f(O_2)$ above the latter, rhodonite becomes unstable and alters to a mixture of braunite and quartz according to the reaction:

$$\text{braunite + quartz = rhodonite} + O_2 \qquad (1)$$

TABLE 4. REPRESENTATIVE COMPOSITIONS OF PYROXENOIDS AND CLINOPYROXENE

Sample Mineral	G39-917 Rdn	G64-740 Rdn	G109-88 Rdn	G76-496 Pxm	G118-188 Cpx	G39-917 Cpx	G109-88 Cpx
SiO_2 wt.%	47.12	47.46	47.49	47.04	50.43	51.31	52.48
TiO_2	n.d.	n.d.	n.d.	n.d.	n.d.	n.d.	n.d.
Al_2O_3	n.d.	n.d.	n.d.	n.d.	0.07	n.d.	n.d.
Fe_2O_3*	0.36	0.24	n.d.	1.86	0.75	0.67	2.54
FeO	5.98	1.27	2.58	4.70	15.83	14.21	12.64
MnO	39.48	41.78	41.78	40.49	7.48	9.88	9.02
MgO	1.84	2.70	2.05	4.32	6.14	5.40	7.09
CaO	5.13	5.63	5.93	1.53	18.90	17.29	14.57
ZnO	0.62	1.28	n.d.	1.00	0.14	0.19	0.19
Na_2O	n.d.	n.d.	n.d.	n.d.	0.35	1.12	2.05
Total	100.52	100.37	99.83	100.93	100.09	100.08	100.58
Si *apfu*	1.994	1.996	2.008	1.971	2.001	2.033	2.040
Ti	0.000	0.000	0.000	0.000	0.000	0.000	0.000
Al	0.000	0.000	0.000	0.000	0.003	0.000	0.000
Fe^{3+}	0.012	0.007	0.000	0.059	0.022	0.020	0.074
Fe^{2+}	0.211	0.045	0.091	0.165	0.525	0.471	0.411
Mn	1.415	1.488	1.496	1.437	0.251	0.332	0.297
Mg	0.116	0.170	0.129	0.270	0.363	0.319	0.411
Ca	0.232	0.254	0.269	0.069	0.803	0.734	0.607
Zn	0.019	0.040	0.000	0.031	0.004	0.006	0.005
Na	0.000	0.000	0.000	0.000	0.027	0.086	0.154
$FeSiO_3$	11.2	2.7	4.6	11.2	-	-	-
$MnSiO_3$	71.2	75.8	75.4	71.9	-	-	-
$MgSiO_3$	5.8	8.6	6.5	13.5	-	-	-
$CaSiO_3$	11.7	12.9	13.5	3.4	-	-	-
Hedenbergite	-	-	-	-	47.1	43.0	40.7
Diopside	-	-	-	-	31.3	27.9	34.4
Johannsenite	-	-	-	-	21.6	29.0	24.9

Notes: n.d.: not detected. * The proportion of Fe_2O_3 is calculated from stoichiometry. Results of all analyses were normalized to six atoms of oxygen; cation proportions are expressed in atoms per formula unit (*apfu*). Proportions of the components are expressed in mol.%. Symbols: Rdn: rhodonite, Pxm: pyroxmangite, Cpx: clinopyroxene.

TABLE 5. CHEMICAL COMPOSITION OF ASSOCIATED MINERALS

Sample Mineral	G38-1080 cal	G38-1080 tr	G38-1080 mtk	G79-496 pyf	GR-65 ep	G111-284 kfs	G109-88 kfs
SiO_2 wt.%	-	55.19	15.82	0.05	33.24	55.55	65.43
TiO_2	-	n.d.	1.16	51.28	n.d.	n.d.	0.39
Al_2O_3	-	0.49	0.27	n.d.	17.31	20.23	17.29
Fe_2O_3*	-	-	17.22	3.32	16.22	-	-
FeO	n.d.	2.32	-	0.96	-	n.d.	0.16
MnO	10.38	11.41	0.72	44.22	1.74	-	-
MgO	n.d.	19.12	0.15	n.d.	0.05	-	-
CaO	47.27	6.37	n.d.	n.d.	11.44	-	-
ZnO	n.d.	1.40	0.12	0.48	n.d.	-	-
Na_2O	-	0.35	-	-	-	1.92	1.37
K_2O	-	n.d.	-	-	-	8.90	14.36
PbO	n.d.	-	63.99	-	1.37	n.d.	n.d.
BaO	n.d.	-	0.10	-	n.d.	13.47	0.82
SrO	n.d.	-	-	-	15.83	n.d.	n.d.
CO_2*	43.60		-	-	-	-	-
Total	101.25	96.65	99.54	100.31	97.21	100.07	99.82
Si *apfu*	-	7.948	1.992	0.003	2.996	2.783	3.026
Ti	-	0.000	0.110	1.935	0.000	0.000	0.014
Al	-	0.083	0.040	0.000	1.839	1.194	0.943
Fe^{3+}	-	0.000	1.631	0.125	1.100	-	-
Fe^{2+}	0.000	0.279	-	0.040	-	0.000	0.006
Mn	0.296	1.392	0.077	1.879	0.133	-	-
Mg	0.000	4.105	0.028	0.000	0.003	-	-
Ca	1.702	0.983	0.000	0.000	1.105	-	-
Zn	0.000	0.171	0.011	0.018	0.000	-	-
Na	-	0.098	-	-	-	0.186	0.123
K	-	0.000	-	-	-	0.569	0.847
Pb	0.000	-	2.169	-	0.033	0.000	0.000
Ba	0.000	-	0.005	-	0.000	0.264	0.015
Sr	0.000	-	-	-	0.827	0.000	0.000
C	2.001	-	-	-	-	-	-

Notes: -: not analyzed, n.d.: not detected. * The proportion of Fe_2O_3 and CO_2 is calculated from stoichiometry. Results of analyses were normalized to six atoms of oxygen for calcite (cal) and pyrophanite (pyf), eight atoms for K-feldspar (kfs), nine atoms for melanotekite (mtk), 12.5 atoms for epidote (ep), and 23 atoms for tremolite (tr); cation proportions are expressed in atoms per formula unit (*apfu*).

The close spatial association of both hematite- and magnetite-bearing assemblages suggests oxygen fugacities close to the HM buffer. This evidence is in agreement with experimental studies on the stability of calderite, which indicate stability only under a limited range of oxygen fugacities close to the HM and Cu–Cu_2O buffers (Lattard & Schreyer 1983). At slightly higher $f(O_2)$ conditions, equivalent to the Cu_2O–CuO buffer, calderite was found to coexist with braunite, hematite and quartz, and becomes totally replaced by more oxygenated phases at even higher oxygen fugacities. A lower limit of $f(O_2)$ is suggested by the breakdown of calderite to a mixture of olivine, pyroxmangite and magnetite at oxygen fugacities equivalent to the Ni–NiO buffer (Lattard & Schreyer 1983). These considerations place the ambient $f(O_2)$ between 10^{-7} and 10^{-13} bars for assemblages containing garnet + hematite and between 10^{-12} and 10^{-17} bars for those containing garnet + magnetite (Fig. 11).

The presence of a considerable proportion of the magnetite component in spinel of type (i) assemblages suggests that $f(O_2)$ was below the HM buffer. As shown by Johnson *et al.* (1990), however, dilution of magnetite by franklinite may shift the HM equilibrium to slightly higher $f(O_2)$. A lower limit is given by the Ni–NiO buffer based on the stability of coexisting calderite (Lattard & Schreyer 1983).

Discussion and Conclusions

Experimental studies on Mn-rich phases have been conducted under various P–T–$f(O_2)$ conditions. Huebner (1967) investigated the system Mn–Si–C–O and determined the stability field of rhodochrosite. The systems Mn–Si–O and Mn–Si–Al–O were studied by Abs-Wurmbach *et al.* (1983) and Abs-Wurmbach & Peters (1999), respectively. Phase relations of Fe- and Mn-rich rocks were investigated by Dasgupta & Manickavasagam (1981) for parts of the system Mn–Fe–Si–O, and by Dasgupta *et al.* (1989) for the system Mn–Fe–Si–C–O. The stability of calderite in the system Fe–Mn–Si–O was determined by Lattard & Schreyer (1983). These studies resulted in the construction of petrogenetic grids for a variety of Mn-rich silicate, carbonate and oxide phases, and various reactions have been proposed to account for the observed assemblages of minerals in natural deposits. In contrast, phase relations in the system Fe–Mn–Zn–O are poorly constrained owing to a lack of experimental data. Valentino *et al.* (1990) investigated miscibility along the franklinite–magnetite join, whereas Beard & Tracy (2002) provided field evidence of solvus relations between jacobsite and magnetite. These investigators suggested that a complete solid-solution exists among magnetite, franklinite and jacobsite at temperatures above 500°C.

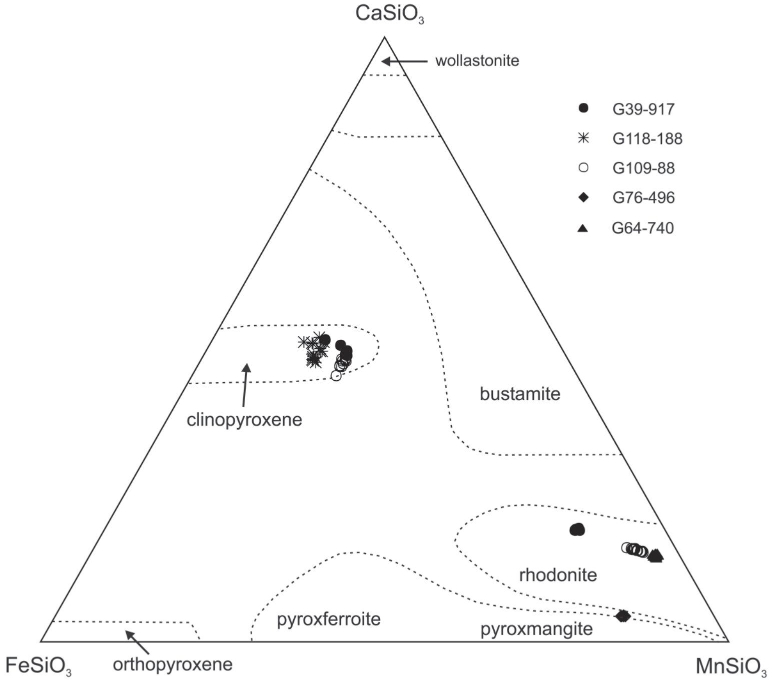

FIG. 9. Composition of pyroxenoids and clinopyroxene in terms of the $FeSiO_3$–$MnSiO_3$–$CaSiO_3$ diagram. Single-chain silicate fields after Brown *et al.* (1980).

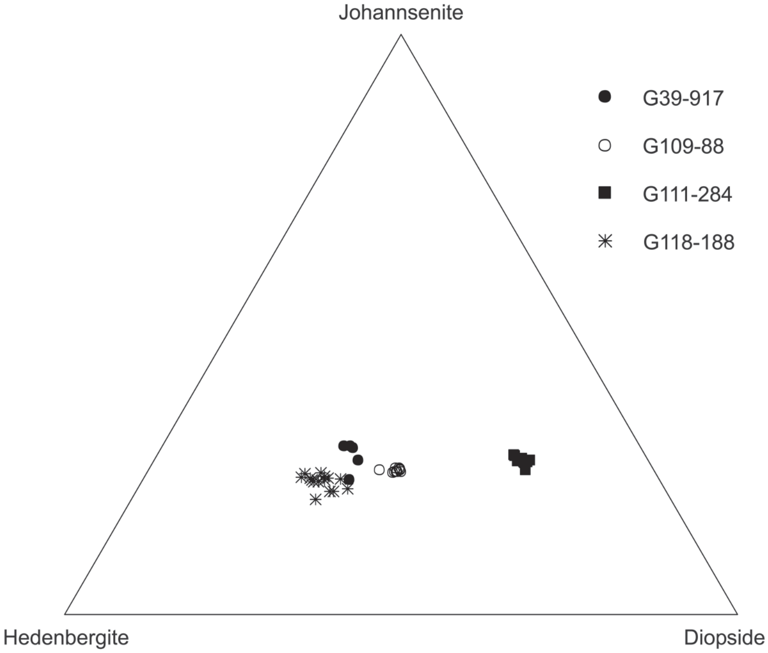

FIG. 10. Composition of clinopyroxene in terms of the hedenbergite – diopside – johannsenite plot.

The observed assemblages of minerals in metamorphosed manganiferous sediments are a function of P, T, bulk composition, $f(O_2)$ and the nature of the fluid phase. Dasgupta *et al.* (1990) and Dasgupta (1997) demonstrated that Mn silicate rocks develop through reduction or decarbonation reactions from primary Mn-oxide-rich or Mn-carbonate-rich precursors. At Gamsberg, the preservation of carbonate in some samples and the presence of Fe^{3+}-rich minerals suggest that the metasediments were derived from Mn–Ca carbonate admixed with varying amounts of Fe-rich oxides, hydroxides and silica. Contamination of these chemical sediments with varying amounts of detrital aluminous clays resulted in layer-to-layer variation of the andradite, calderite and spessartine component of garnet. Most investigators have proposed the reaction

Mn-rich chlorite + quartz = spessartine + H_2O (2)

to account for the appearance of spessartine in a variety of metamorphosed Mn-silicate rocks (*e.g.*, Ashley 1989, Dasgupta 1997). The formation of andradite- and calderite-rich garnet requires additional Fe^{3+}, Mn and Ca, which were most probably derived from primary oxides and carbonate. Under the P–T and $f(O_2)$ conditions experienced at Gamsberg, the distribution of andradite–calderite-rich *versus* spessartine-rich garnet was primarily controlled by bulk composition, especially the (Mn + Ca)/Al value. As Fe^{3+} and Mn were readily available in the precursor sediments, the calderite-rich garnet developed in samples where a deficiency in Al prevented incorporation of all the Mn into spessartine.

Experimental studies by Lattard & Schreyer (1983) have shown that end-member calderite is stable only under very high pressures (>22 kbar) and low temperatures, equivalent to conditions encountered in subduction zones. However, dilution of calderite by spessartine or andradite or both expands the stability field to considerably lower pressures and can explain the presence of such garnet in regionally metamorphosed terranes. At Gamsberg, textural and chemical relationships discussed earlier indicate that calderitic garnet was altered to clinopyroxene in some assemblages. The equilibrium between Fe-rich clinopyroxene and andraditic garnet is given by the reaction (Burton *et al.* 1982):

hedenbergite + O_2 = andradite
+ magnetite + quartz (3)

At conditions of 700°C and P = 2 kbar, the hedenbergite–andradite equilibrium lies at $f(O_2)$ of 10^{-15}, thus at conditions between the HM and Ni–NiO buffers. As shown by Burton *et al.* (1982), dilution of hedenbergite by 15 mole % johannsenite raises the stability field of hedenbergite by 1.0 log $f(O_2)$ relative to andradite. Taking the stability of calderite into consideration (Lattard & Schreyer 1983), the breakdown of the garnet was probably controlled by a decrease in pressure during retrograde metamorphism. The stable coexistence of clinopyroxene with andradite–calderite garnet in some assemblages (*e.g.*, G111–284), however, indicates that $f(O_2)$ must have been very close to the equilibrium of these minerals.

The appearance of rhodonite in metamorphosed manganiferous sediments is usually attributed to the decarbonation reaction:

$$\text{rhodochrosite} + \text{quartz} = \text{rhodonite} + CO_2 \qquad (4),$$

as documented by Huebner (1967), Ashley (1989) and Dasgupta (1997).

As shown by Abs-Wurmbach & Peters (1999), high activities of silica are required to stabilize rhodonite or pyroxmangite instead of Mn-rich carbonate or other Mn silicates such as tephroite. Consequently, pyroxenoid is absent in silica-poor samples at Gamsberg (*e.g.*, G38–1080). In Si-rich assemblages such as G77–632 and GR–65, the paragenesis spessartine + quartz + hematite is stabilized instead of andradite–calderite garnet and pyroxenoid.

TABLE 6. BULK COMPOSITION OF SELECTED ASSEMBLAGES

Sample	G38-1080	G74-680	G39-917	G76-496	G64-740	GR-65	G77-632
Type	(i)	(i)	(ii)	(ii)	(iii)	(iii)	(iii)
Paragenesis	grt-spl[1]-cal	grt-spl[1]-rdn	grt-rdn-cal-cpx-mgt	grt-pxm-qtz-mgt	grt-rdn-qtz-hem	grt-qtz-hem-ep	grt-qtz-hem-cal
Garnet type[2]	adr-cld	adr-cld	adr-cld	sps	adr-cld	sps	sps
SiO_2 wt.%	17.55	29.30	36.63	49.00	38.39	47.05	46.33
TiO_2	0.18	0.20	0.25	0.60	0.17	0.44	0.49
Al_2O_3	5.12	2.58	3.06	9.93	3.42	7.69	7.32
Fe_2O_3	28.63	34.18	12.12	13.61	21.62	15.76	21.84
FeO	4.05	-	6.30	-	1.31	-	-
MnO	14.72	15.47	16.82	19.12	21.49	17.64	14.72
MgO	0.17	1.45	1.79	1.33	1.88	0.88	0.70
CaO	17.06	8.54	12.79	2.42	7.93	7.42	4.59
Na_2O	0.25	0.07	0.77	0.09	0.00	0.31	0.09
K_2O	0.03	0.02	1.47	1.40	0.01	0.03	0.30
P_2O_5	0.75	0.63	0.36	0.36	0.27	0.42	0.50
H_2O^-	0.04	1.45	0.24	0.09	0.09	0.23	0.21
LOI	7.11	1.79	4.21	0.15	0.76	0.62	0.00
Total	95.66	95.69	96.81	98.10	97.33	98.49	98.49
Cu ppm	82	n.d.	n.d.	n.d.	n.d.	n.d.	129
Pb	7036	1562	4149	267	3645	79	450
Zn	3973	16414	1592	2716	6756	969	3400
Ba	258	2729	1276	2444	478	657	3828
Sr	4093	610	286	415	640	1020	198
As	111	149	-	-	-	1379	450
Mn/Fe	0.49	0.50	0.97	1.55	1.03	1.24	0.75
Mn/Al	4.21	8.78	8.04	2.82	9.19	3.36	2.94
Fe/Si	2.82	1.75	0.78	0.42	0.90	0.50	0.71
Si/(Si+Mn)	0.42	0.53	0.57	0.61	0.52	0.62	0.66

Notes: -: not analyzed, n.d..: not detected. Symbols: cal: manganoan calcite, cpx: clinopyroxene, ep: epidote, grt: garnet, hem: hematite, mgt: magnetite, pxm: pyroxmangite, qtz: quartz, rdn: rhodonite. 1: Zn–Mn-rich ferrite spinel, 2: adr–cld: andradite–calderite-dominant, sps: spessartine-dominant.

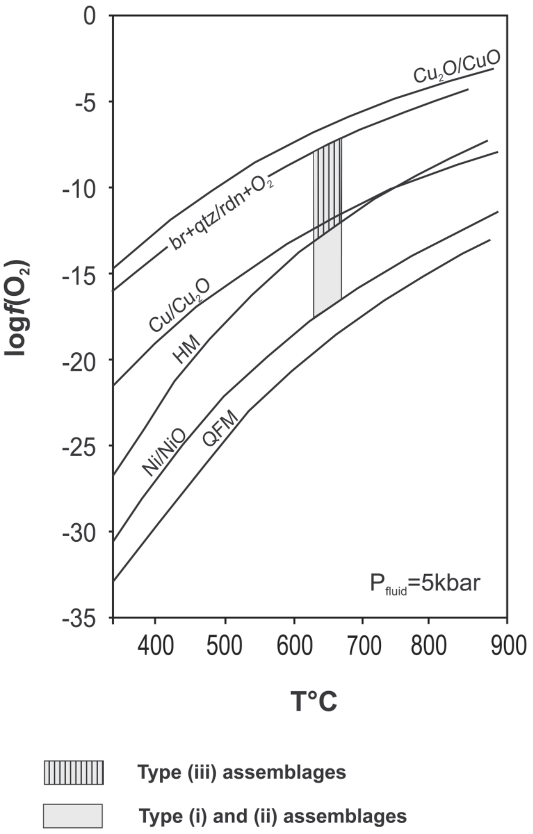

Fig. 11. Log $f(O_2)$–T plot for various buffers of interest. Estimated $f(O_2)$ ranges for the different assemblages under the ambient temperatures of metamorphism are indicated. The buffer curves are from Abs-Wurmbach *et al.* (1983) and Spear (1993). Mineral symbols: br: braunite, qtz: quartz, rdn: rhodonite.

The coexistence of rhodonite with Mn-rich spinel can be explained by the reaction:

$$\text{rhodochrosite} + \text{magnetite} + \text{quartz} = \text{rhodonite} + \text{manganoan magnetite} + CO_2 \qquad (5)$$

(Dasgupta *et al.* 1993).

At Gamsberg, the available Zn in the bulk composition was incorporated into spinel and resulted in a solid solution toward the franklinite end-member. The latter only developed in relatively Si-poor and Fe-rich bulk compositions. More Si- and Mn-rich compositions resulted in the paragenesis magnetite + pyroxenoid, as evident from type (ii) assemblages. In addition, the presence of sufficient Ti in the spinel structure resulted in the unmixing of Mn as pyrophanite.

The contrasting parageneses observed within the C2 unit are interpreted to reflect compositional layering of original metalliferous sediment. Modern metalliferous sediments, such as found in the Red Sea (*e.g.,* Atlantis II Deep) or on the Mid-Atlantic Ridge (*e.g.,* TAG hydrothermal mound) are normally delicately laminated, as manifested by alternating layers of sulfides, silicates, oxides and carbonates. Evidence from these deposits has shown that Fe and Mn are commonly decoupled from the sulfide facies and precipitate peripherally to active high-temperature venting (Anschutz & Blanc 1995, Herzig & Hannington 1995, Goulding *et al.* 1998). We propose that such Mn–Fe-rich hydrothermal material formed a low-temperature, oxidized, dispersion halo around the Gamsberg deposit, therefore favoring a submarine exhalative origin of mineralization. Owing to the sedimentary nature of the protolith, original compositional variations took place over short vertical distances (centimeter to decimeter scale) and resulted in the distinct lamination of the metamorphosed rocks. Metahydrothermal rocks associated with other metamorphosed base-metal sulfide deposits (*e.g.,* Broken Hill and Cannington, in Australia) are relatively more Fe- and Si-rich, and contain units such as oxide- and silicate-facies iron formations and quartz–gahnite rocks (Plimer 1986, Spry *et al.* 2000). The Mn–Fe–Ca-rich nature of metahydrothermal rocks at Gamsberg illustrates the spectrum of rock types that may be associated with Broken-Hill-type mineralization, and therefore provides additional criteria for exploration of this important class of base-metal deposits.

ACKNOWLEDGEMENTS

The authors thank technical personnel at the University of Stellenbosch and Rhodes University, Grahamstown, for their help with sample preparation and analytical procedures. Gary Stevens is thanked for proof reading the manuscript. Critical reviews and constructive comments by Eric Essene and Craig Johnson considerably improved an earlier version of the manuscript. The Department of Geology of the University of Stellenbosch sponsored the project.

REFERENCES

ABS-WURMBACH, I. & PETERS, T. (1999): The Mn–Al–Si–O system: an experimental study of phase relations applied to parageneses in manganese-rich ores and rocks. *Eur. J. Mineral.* **11**, 45-68.

________, ________, LANGER, K. & SCHREYER, W. (1983): Phase relations in the system Mn–Si–O: an experimental and petrological study. *Neues Jahrb. Mineral., Abh.* **146**, 258-279.

ANTHONY, J.W., BIDEAUX, R.A., BLADH, K.W. & NICHOLS, M.C. (1997): *Handbook of Mineralogy.* III. Halides, Hydroxides, Oxides. Mineral Data Publishing, Tucson, Arizona.

ANSCHUTZ, P. & BLANC, G. (1995): Chemical mass balances in metalliferous deposits from the Atlantis II Deep, Red Sea. *Geochim. Cosmochim. Acta* **59**, 4205-4218.

ASHLEY, P.M. (1989): Geochemistry and mineralogy of tephroite-bearing rocks from the Hoskins manganese mine, New South Wales, Australia. *Neues Jahrb. Mineral., Abh.* **161**, 85-111.

BEARD, J.S. & TRACY, R.T. (2002): Spinels and other oxides in Mn-rich rocks from the Hutter mine, Pittsylvania County, Virginia, U.S.A.: implications for miscibility and solvus relations among jacobsite, galaxite, and magnetite. *Am. Mineral.* **87**, 690-698.

BROWN, P.E., ESSENE, E.J. & PEACOR, D.R. (1980): Phase relations inferred from field data for Mn pyroxenes and pyroxenoids. *Contrib. Mineral. Petrol.* **74**, 417-425.

BÜHN, B., OKRUSCH, M., WOERMANN, E., LEHNERT, K. & HOERNES, S. (1995): Metamorphic evolution of Neoproterozoic manganese formations and their country rocks at Otjosondu, Namibia. *J. Petrol.* **36**, 463-496.

BURKE, E.A.J. & KIEFT, C. (1972): Franklinite from Långban, Sweden: a new occurrence. *Lithos* **5**, 69-72.

BURTON, J.C., TAYLOR, L.A. & CHOU, I-MING (1982): The f_{O2}–T and f_{S2}–T stability relations of hedenbergite and of hedenbergite–johannsenite solid solution. *Econ. Geol.* **77**, 764-783.

DASGUPTA, S. (1997): P–T–X relationships during metamorphism of manganese-rich sediments: current status and future studies. *In* Manganese Mineralization: Geochemistry and Mineralogy of Terrestrial and Marine Deposits (K. Nicholson, J.R. Hein, B. Bühn & S. Dasgupta, eds). *Geol. Soc., Spec. Publ.* **119**, 327-337.

________, BANERJEE, H., FUKUOKA, M., BHATTACHARYA, P.K. & ROY, S. (1990): Petrogenesis of metamorphosed manganese deposits and the nature of the precursor sediments. *Ore Geol. Rev.* **5**, 359-384.

__________, BHATTACHARYA, P.K., BANERJEE, H., FUKUOKA, M., MAJUMDAR, N. & ROY, S. (1987): Calderite-rich garnets from metamorphosed manganese silicate rocks of the Sausar Group, India, and their derivation. *Mineral. Mag.* **51**, 577-583.

________ & MANICKAVASAGAM, R.M. (1981): Regional metamorphism of non-calcareous manganiferous sediments from India and the related petrogenetic grid for a part of the system Mn–Fe–Si–O. *J. Petrol.* **22**, 363-396.

________, SENGUPTA, P., BHATTACHARYA, P.K., MUKHERJEE, M., FUKUOKA, M., BANERJEE, H. & ROY, S. (1989): Mineral reactions in manganese oxide rocks: P–T–X phase relations. *Econ. Geol.* **84**, 434-443.

________, ________, FUKUOKA, M. & ROY, S. (1993): Contrasting parageneses in the manganese silicate–carbonate rocks from Parseoni, Sausar Group, India and their interpretation. *Contrib. Mineral. Petrol.* **114**, 533-538.

DROOP, G.T.R. (1987): A general equation for estimating Fe^{3+} concentrations in ferromagnesian silicates and oxides from microprobe analyses, using stoichiometric criteria. *Mineral. Mag.* **51**, 431-435.

FRONDEL, C. & KLEIN, C., JR. (1965): Exsolution in franklinite. *Am. Mineral.* **50**, 1670-1680.

GLASSER, F.P. (1967): New data on kentrolite and melanotekite: ternary phase relations in the system PbO–Fe_2O_3–SiO_2. *Am. Mineral.* **52**, 1085-1093.

GOULDING, H.C., MILLS, R.A. & NESBITT, R.W. (1998): Precipitation of hydrothermal sediments on the active TAG mound: implications for ochre formation. *In* Modern Ocean Floor Processes and the Geological Record (R.A. Mills & K. Harrison, eds.). *Geol. Soc., Spec. Publ.* **148**, 201-216.

GRAPES, R.H. & WATANABE, T. (1984): Al–Fe^{3+} and Ca–Sr^{2+} epidotes in metagreywacke–quartzofeldspathic schist, Southern Alps, New Zealand. *Am. Mineral.* **69**, 490-498.

HERZIG, P.M. & HANNINGTON, M.D. (1995): Polymetallic massive sulfides at the modern seafloor: a review. *Ore Geol. Rev.* **10**, 95-115.

HITZMAN, M.W., REYNOLDS, N.A., SANGSTER, D.F., ALLEN, C.R. & CARMAN, C.E. (2003): Classification, genesis, and exploration guides for nonsulfide zinc deposits. *Econ. Geol.* **98**, 685-714.

HOLTSTAM, D. (2002): New occurrences of willemite–franklinite assemblages in Bergslagen, central Sweden. *Eur. J. Mineral.* **14**, 621-626.

HUEBNER, J.S. (1967): *Stability Relations of Minerals in the System Mn–Si–C–O.* Ph.D thesis, John Hopkins Univ., Baltimore, Maryland.

JIMÉNEZ-MILLÁN, J. & VELILLA N. (1994): Mineralogy and geochemistry of reduced manganese carbonate–silicate rocks from the Aracena area (Iberian Massif, SW Spain). *Neues Jahrb. Mineral., Abh.* **166**, 193-209.

JOHNSON, C.A., RYE, D. & SKINNER, B.J. (1990): Petrology and stable isotope geochemistry of the metamorphosed zinc–iron–manganese deposit at Sterling Hill, New Jersey. *Econ. Geol.* **85**, 1133-1161.

________ & SKINNER, B.J. (2003): Geochemistry of the Furnace magnetite bed, Franklin, New Jersey, and the relationship between stratiform iron oxide ores and stratiform zinc-oxide–silicate ores in the New Jersey Highlands. *Econ. Geol.* **98**, 837-854.

JOUBERT, P. (1986): The Namaqualand Metamorphic Complex – a summary. *In* Mineral Deposits of Southern Africa II (C.R. Anhaeusser & S. Maske, eds.). Geological Society of South Africa, Johannesburg, South Africa (1395-1420).

KLEIN, C., JR. (1966): Mineralogy and petrology of the metamorphosed Wabush iron formation, southwestern Labrador. *J. Petrol.* **7**, 246-305.

LATTARD, D. & SCHREYER, W. (1983): Synthesis and stability of the garnet calderite in the system Fe–Mn–Si–O. *Contrib. Mineral. Petrol.* **84**, 199-214.

MOORE, J.M., WATKEYS, M.K. & REID, D.L. (1990): The regional setting of the Aggeneys/Gamsberg base metal deposits, Namaqualand, South Africa. *In* Regional Metamorphism of Ore Deposits (P.G. Spry & L.T. Bryndzia, eds.). VNU Science Press, Rotterdam, the Netherlands (77-95).

PLIMER, I.R. (1986): Sediment-hosted exhalative Pb–Zn deposits – products of contrasting ensialic rifting. *Trans. Geol. Soc. S. Afr.* **89**, 57-73.

REINECKE, T. (1987): Manganoan deerite and calderitic garnet from high-pressure metamorphic Fe–Mn-rich quartzites on Andros Island, Greece. *Mineral. Mag.* **51**, 247-251.

ROBB, L.J., ARMSTRONG, R.A. & WATERS, D.J. (1999): The history of granulite-facies metamorphism and crustal growth from single zircon U–Pb geochronology: Namaqualand, South Africa. *J. Petrol.* **40**, 1747-1770.

ROZENDAAL, A. (1986): The Gamsberg zinc deposit, Namaqualand District. *In* Mineral Deposits of Southern Africa II (C.R. Anhaeusser & S. Maske, eds.). Geological Society of South Africa, Johannesburg, South Africa (1477-1488).

________ & STUMPFL, E.F. (1984): Mineral chemistry and genesis of Gamsberg zinc deposit, South Africa. *Trans. Inst. Mining Metall. (Sect. B: Appl. Earth Sci.)* **93**, B161-175.

SCLAR, C.B. & LEONARD, B.F. (1992): Quantitative chemical relationships in a franklinite–magnetite exsolution intergrowth from Franklin, Sussex County, New Jersey. *Econ. Geol.* **87**, 1180-1183.

SPEAR, F.S. (1993): *Metamorphic Phase Equilibria and Pressure – Temperature – Time Paths.* Mineralogical Society of America, Washington, D.C.

SPRY, P.G., PETER, J.M. & SLACK, J.F. (2000): Meta-exhalites as exploration guides to ore. *In Metamorphosed and Metamorphogenic Ore Deposits* (P.G. Spry, B. Marshall & F.M. Vokes, eds.). *Rev. Econ. Geol.* **11**, 163-201.

STALDER, M. & ROZENDAAL, A. (2002): Graftonite in phosphatic iron formations associated with the mid-Proterozoic Gamsberg Zn–Pb deposit, Namaqua Province, South Africa. *Mineral. Mag.* **66**, 915-927.

________ & ________ (2004): Apatite nodules as an indicator of depositional environment and ore genesis for the Mesoproterozoic Broken Hill-type Gamsberg Zn–Pb deposit, Namaqua Province, South Africa. *Mineral. Deposita* **39**, 189-203.

THOMAS, R.J., AGENBACHT, A.L.D., CORNELL, D.H. & MOORE, J.M. (1994): The Kibaran of southern Africa: tectonic evolution and metallogeny. *Ore Geol. Rev.* **9**, 131-160.

VALENTINO, A.J., CARVALHO, A.V., III & SCLAR, C.B. (1990): Franklinite – magnetite – pyrophanite intergrowths in the Sterling Hill zinc deposit, New Jersey. *Econ. Geol.* **85**, 1941-1946.

Received May 8, 2003, revised manuscript accepted December 8, 2004.